npj | climate and atmospheric science

Article

Published in partnership with CECCR at King Abdulaziz University

https://doi.org/10.1038/s41612-026-01519-0

Hail trajectories under climate change: disentangling the roles of moisture, melting level and updraft kinematics

Check for updates

Jannick Fischer[1] ✉, Matthew R. Kumjian[2], Yuzhu Lin[3] & Kelly Lombardo[2]

Large hail is expected to become more frequent under climate change. However, uncertainties remain because storm dynamics and hail formation are imperfectly captured by environmental hail proxies and in convection-permitting models, which are the two most frequently used approaches. We address this using a nonspherical hail-trajectory model in an ensemble of 171 idealized cloud model simulations. Melting level, cloud water, updraft intensity, and updraft width are varied independently. The results largely confirm previous work: rising melting levels (+3-K warming) reduce hail size spectra via enhanced melting and shorter residence times, but increased cloud water dominates, yielding a 30–40% rise in >2-cm hail and 25% larger hail area. However, changes in updraft intensity/width exert stronger, non-monotonic effects, underscoring critical uncertainties and the need to integrate storm structure and robust hail diagnostics in future research.

Global damage from severe convective storms and particularly from hail is increasing, which can in part be attributed to climate change[1]. This finding is largely based on a number of studies examining changes in the atmospheric environmental ingredients as proxies for hail [2–6]. As reviewed by Ref. 7, increasing temperatures lead to higher environmental water vapor content, allowing more condensate and latent heat to be released in convective updrafts and producing more intense storms with higher liquid water contents. At the same time, higher temperatures raise the melting level, leading to increased melting, especially of small hail before it reaches the ground. Taken together, these factors suggest that convective storms produce less frequent hail, but more severe hail in a warmer climate. However, a few recent studies have pointed out that trends in the atmospheric environments needed for hail can be misleading, because of biases in climate models and reanalyses or because the physical processes, initiation, and structure of hailstorms could adjust in ways not represented by data-driven models[8–10].

An important alternative approach has recently evolved with computationally-expensive convection-permitting climate simulations. Ref. 11 compared parameterized hail production in simulated storms over 15-year periods for historical, mid-century, and end-of-century climate conditions over the USA and found a decrease in the surface frequency of small and severe hail (we will use the terminology of[12], defining "small," "severe," "significantly severe," and "giant" for hail sizes <2.5 cm, 2.5-5 cm, 5-10 cm, and >10 cm, respectively) and an increase for larger sizes. For Europe[13], a sophisticated one-dimensional hail growth model was used in 11-year convection-permitting simulations, and a reduction in the frequency of hail <1.25 cm and an increase in larger hail were found. In contrast, Ref. 14 reported a general decrease in hail frequency, with the exception of significantly severe hail. Overall, these studies broadly align with the physical expectations reviewed by Ref. 7 and with previous convection-permitting climate simulation studies[15,16], but they disagree on the range of hail sizes that are decreasing or increasing in frequency and on whether enhanced melting or stronger convective inhibition is the dominant physical reason driving the decrease. Furthermore, simulations of selected events and regions suggest that the effect of climate change on hail depends on the region and season[17–20].

These uncertainties in the details demonstrate how difficult it is to account for all dynamical and thermodynamic factors that influence hail under climate change. For example, supercells are the main storm type responsible for significantly severe hail[21], as their updraft intensity and structure support hail trajectories with long residence times in the hail growth zone[22,23]. Convection-permitting simulation studies can misrepresent intensity and structure of real storm updrafts due to their still relatively coarse resolution[24,25]. In addition, these studies do not explicitly simulate hail growth and therefore rely on assumptions in their hail diagnostics, often making detailed assessments impossible, such as the full hail size spectrum or the area affected by a hailstorm. In this context, one recommendation by Ref. 7 was "To untangle how climate change may affect hailstorms, and to better compare studies, observed changes in environmental conditions must be tied to their effects on hail through detailed studies of the microphysical chain of events leading to hail production within the storm and the hail that ultimately falls to the ground."

[1]Institute of Meteorology and Climate Research, Karlsruhe Institute of Technology, Karlsruhe, Germany. [2]Department of Meteorology and Atmospheric Science, The Pennsylvania State University, University Park, PA, USA. [3]National Center for Atmospheric Research, Boulder, CO, USA. ✉e-mail: jannick.fischer@kit.edu

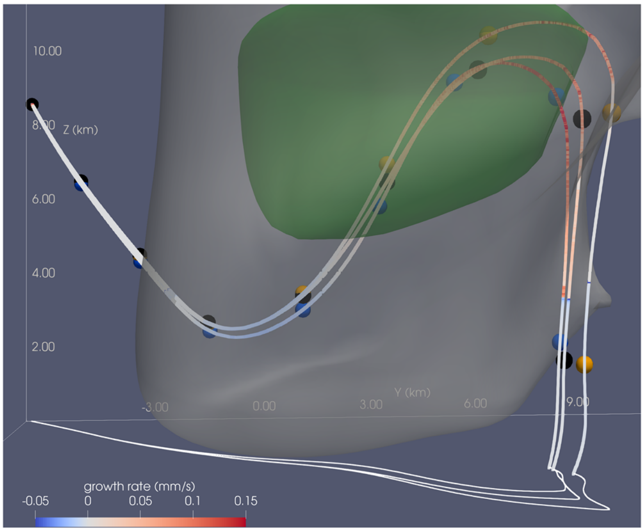

Fig. 1 | Trajectory examples. Examples of trajectories of the same hail embryo in three different simulations of the ensemble (1) the control run referred to in the text (black circles), (2) the 3-K warmer simulation (orange), (3) the 2-g kg−1 moister simulation (blue). The circles are spaced every 3 min along the trajectories. The gray contour shows 3 m s^{-1} updraft and the green contour the 7 g kg^{-1} cloud water mixing ratio in the updraft core of the control run. Color shading indicates growth rate (or melting rate for negative values). The embryo was chosen as a representative example for the hail growth mechanisms discussed in the results. See F25 for more details on the variety of trajectory pathways in these idealized simulations.

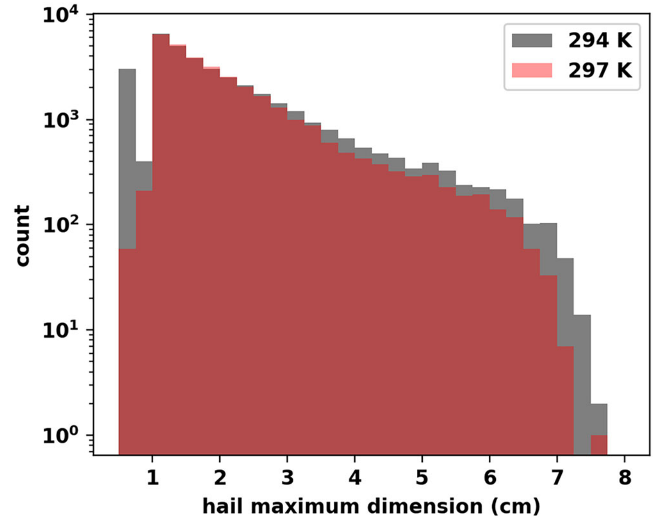

Fig. 2 | Example hail size distribution. Hail size distributions from the hail trajectory model for two example simulations with surface potential temperatures of 294 K and 297 K. The updrafts and input water vapor mass fractions were identical (moderately intense and wide updraft and 13 g kg^{-1}). The size bins are 0.25 cm, i.e., the first bin is 0.5-0.75 cm and so on (graupel sizes were omitted).

The present study takes a step in this direction by using high-resolution cloud model simulations and a detailed three-dimensional nonspherical hail trajectory model. We aim to (i) increase the robustness of trends in hail size and area under climate change by providing an additional perspective compared to the existing literature above and to (ii) elucidate the physical processes that are changing in hailstorms and why they are important. To this end, the roles of the most impactful climate-change-related factors for hail formation - melting level height, cloud water content, updraft intensity, and updraft width - are investigated independently in an ensemble of 171 idealized supercell-like updrafts.

Results

Individual effects on the hail size distribution

The methods described below produce 171 simulations with steady-state supercell-like updrafts based on [Ref. 26, hereafter F25]. The parameters melting level (i.e., five temperature steps in 3-K increments), water vapor mass fraction (five steps in 2-g kg^{-1} increments), updraft intensity, and updraft width are varied independently over ranges expected in midlatitude supercell storms. Subsequently, the detailed nonspherical hail trajectory model runs a grid of 108 732 trajectories upwind of the updraft for each case. As an example, Fig. 1 shows the trajectories of the same hail embryo in three different simulations (the control run used below, a 3-K warmer simulation, and a 2-g kg^{-1} moister simulation). We will come back to these trajectories later, but for now Fig. 1 illustrates that complex three-dimensional trajectories as well as growth and melting are represented. Figure 2 shows the full surface hail size distributions for the control run and a 3-K colder simulation. The size distributions in general are realistic with the exception of a gap in the distribution around 0.8 cm, which is discussed below. Notably, the hail size distribution changes, with fewer hailstones in most size bins for the warmer simulation.

By calculating the difference between these hail size spectra, we can quantify how a melting level increase (caused by 3-K warming) affects the hail size distribution (Fig. 3a). Each dot in Fig. 3a represents the relative difference between two simulations with 3 K increasing temperature in the ensemble. Similarly, Fig. 3b–d show differences in the hail spectrum between simulations with only changing water vapor mixing ratio, updraft width, and updraft intensity, respectively. Relative differences are shown instead of absolute differences to facilitate comparison of all sizes. A few points need to be kept in mind when interpreting these plots: (i) The relative differences sometimes become very large when only a few hailstones of the respective size range are produced in one of the compared simulations. Therefore, only data points with a minimum of 10 stones per size bin are included, which is why fewer dots are shown with larger hail size. This reduces the spread in relative changes without influencing the overall results. (ii) Relative differences skew the scale of the y-axis, so increases and decreases become more difficult to compare visually. For example, a doubling of the hailstone count in a given size range (value of 1.0) is not the same as a value of -1.0, which is a reduction by 100% to an absolute count of zero.

That said, Fig. 3a shows that an increase in the temperature profile by 3 K causes a reduction in hail of most sizes. Hail between 0.5 and 1 cm is reduced the most, up to -100% in some simulations (the warmest simulations do not produce any hail smaller than 1 cm). Hail between 1 and 2 cm shows only minor differences and no mean change. Above 3 cm, the average reduction stays relatively constant at around −30% per 3-K warming. Outliers are associated with small absolute numbers. For example, the highest average increase by 70% occurs when the number of hailstones between 5.25 and 5.5 cm increases from 11 to 19 while neighboring size bins do not show an increase. Thus, outliers seem to occur by chance and carry no physical meaning.

As expected, increasing water content by 2 g kg^{-1} has the opposite effect to increasing temperatures for most sizes (Fig. 3b). Only hail below 1 cm shows a decrease with increasing moisture, while there are mean increases by over 100%, especially for significantly severe hail. However, there is also a large spread, especially when approaching giant hail size.

The impacts of updraft width and intensity are consistent with F25. Updraft width has a large positive effect on the amount of hail of most sizes, similar or larger in magnitude than for changing moisture content and with even larger spread. In contrast, updraft intensity shows a diverging signal. Initially weak updrafts (light gray dots) produce more severe hail when their updraft is intensified. However, if the updraft already has optimal intensity (dark gray), further increase in the vertical velocity leads to a reduction of severe hail and larger. This negative trend dominates in Fig. 3d because only size bins with at least 10 hailstones are shown, so many of the weak updraft statistics were excluded. Thus, the average of the boxplot is artificially

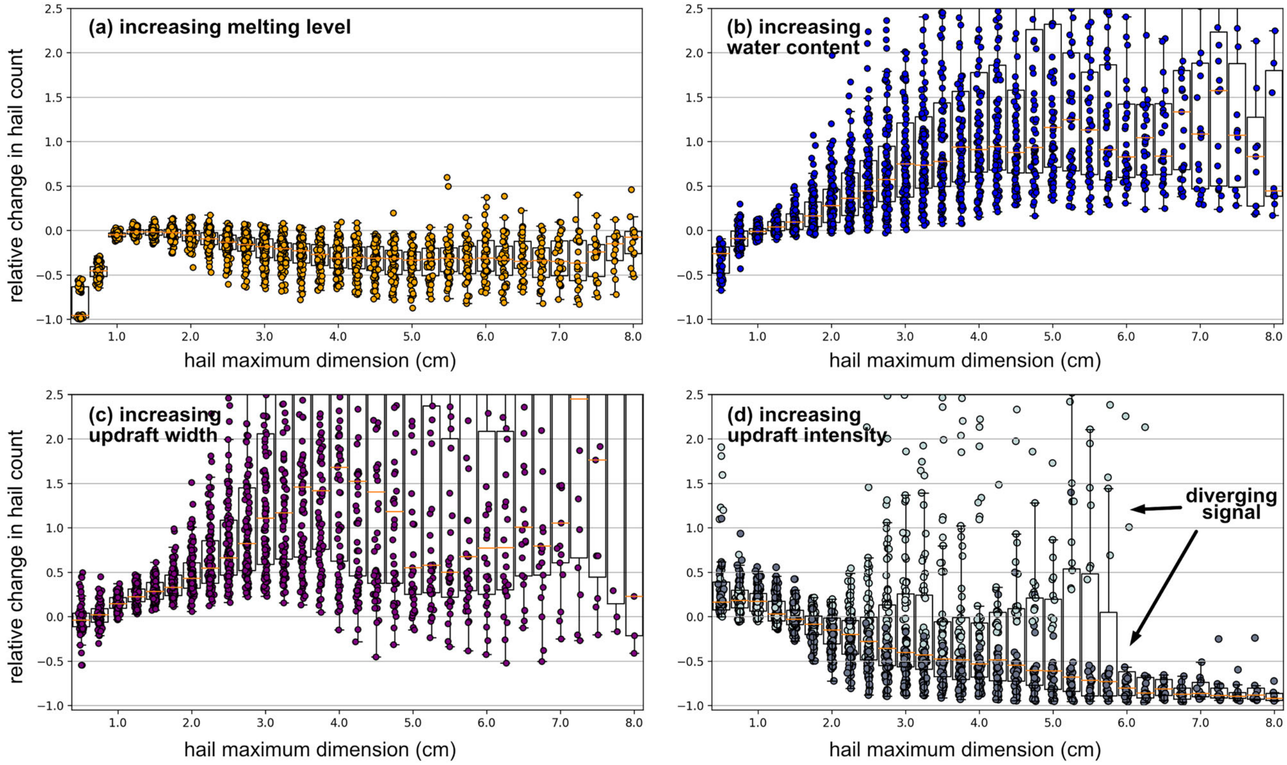

Fig. 3 | Individual changes in the hail size distributions. Each dot per size bin shows the relative difference in hail count from a simulation to the **a** next 3-K warmer simulation, **b** next 2-g kg^{-1} moister simulation, **c** next wider updraft, **d** next more-intense updraft. The size bins are 0.25 cm, i.e., the first bin is 0.5–0.75 cm and so on (graupel sizes were omitted). The underlying boxplots provide the customary information about the distribution. The shading in **d** indicates if the intensity of the initial updraft was low (light gray) or moderate (dark gray). In all plots, the axes were cropped to the same range to allow for comparability and because outliers were often unrealistic due to the calculation of relative differences (see text).

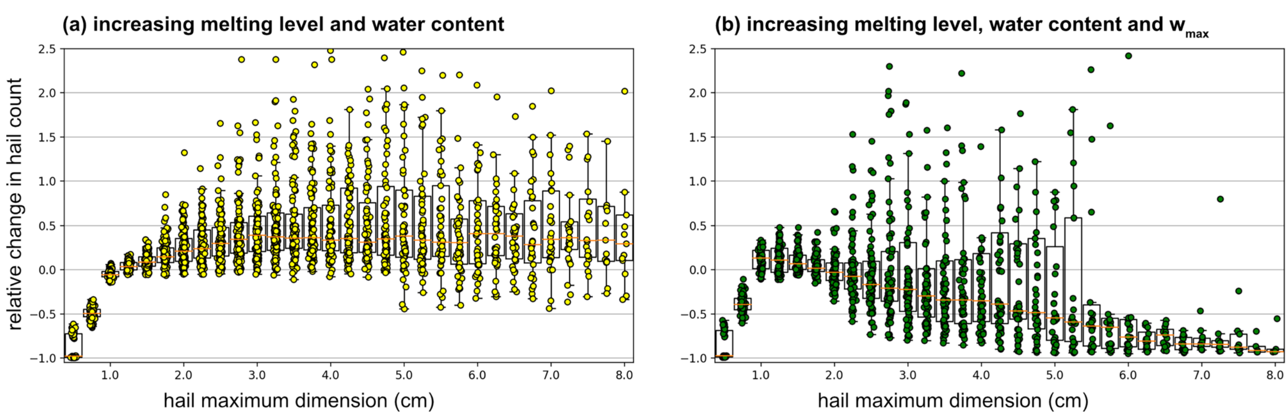

Fig. 4 | Combined changes in the hail size distributions. As Fig. 3, but for relative hail count differences between **a** simulations with both increasing temperature and water vapor mixing ratio and **b** the two of the above and updraft intensity.

skewed toward the stronger updraft, so the negative signal is not a robust result. As discussed in more detail below, these results for the updraft kinematics point to the importance and complexity of changes in storm type and structure with climate change, which are poorly understood and outside the scope of this study.

Combined effects and link to climate change

More relevant perhaps is the question of what the individual results found above can tell us about real climate change. In a warming world, it has been shown that storm environments approximately follow the Clausius-Clapeyron (CC) scaling, meaning that near-ground water vapor mixing ratios increase by around 7% per degree warming[27]. We can account for this simultaneous change by calculating the differences in the hail size distribution between simulations in which both temperature and water vapor are increasing by one increment (Fig. 4a). Since the temperature increments are 3 K between simulations and water vapor mixing ratio increments are 2 g kg^{-1} between values of [9, 11, 13, 15, 17] g kg^{-1}, this means that the mixing ratios increase by 4–7% per degree warming (13–22% per 3-K warming depending on the mixing ratio) when comparing two of the simulations in this way. Thus, CC scaling is on the conservative side, which we keep in mind when interpreting the results. In other words, relative humidity near the ground is not held constant. Since some regions of the world are becoming drier[13], this variability in CC scaling in our ensemble may help to quantify some of the uncertainty.

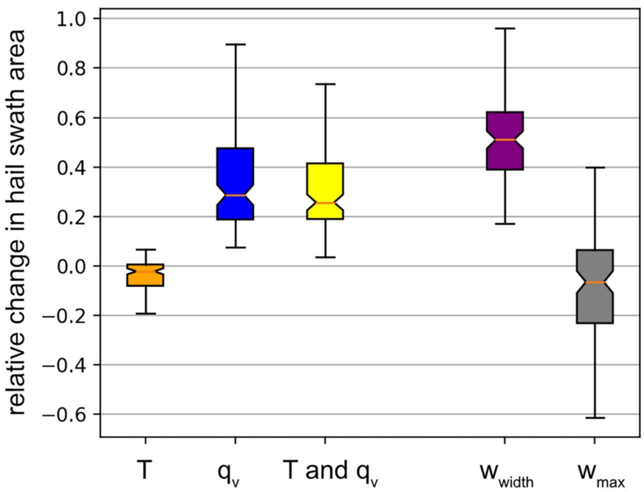

Fig. 5 | Relative change in the hail swath area. Each box shows the distribution of relative differences between simulations with only increasing melting level (i.e., temperature in 3-K increments; orange), water content (2-g kg−1 increments; blue), both (yellow), updraft width (purple) and updraft intensity (gray). Hail swath area was approximated as the number of gridpoints with at least 5 hailstones with a maximum dimension of at least 2 cm.

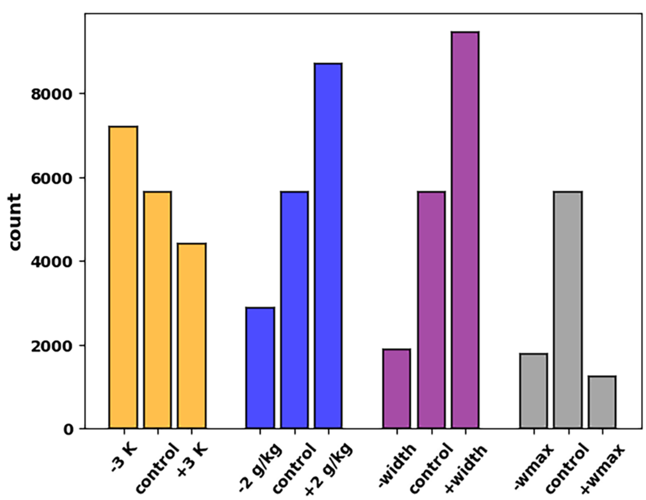

Fig. 6 | Hailstone counts. For each of the simulations analyzed in depth (see text), the number of hailstones with at least 3 cm in maximum dimension is shown. This corresponds to the trajectories analyzed in Fig. 7.

Figure 4 a shows these combined results of increasing melting level height and cloud water content on the hail size spectrum. Changes are positive above 1 cm and negative below, as is expected when combining the signals in Fig. 3a and b. Assuming that the climate change signal lies within the interquartile range of the boxplots, the results suggest that an identically intense supercell updraft in a 3-K warmer and accordingly moister environment will produce less hail <1 cm (-50 to -100% with 3-K warming) and more hail >1.5 cm (+20 to +80% on average in the reliable size range, up to around 9 cm where only a few simulations remain a sufficiently large sample size to be included). These opposing signals for very small and severe hail are consistent with the dichotomy found in previous studies[7,11].

As mentioned in the introduction, updraft intensity is also expected to increase because more condensate and latent heating is released in a warmer environment. Therefore, Fig. 4b shows hail size distribution changes for simulations with increasing temperature, water vapor, and updraft intensity. The diverging signal shown in Fig. 3d also dominates here, so no clear trend can be inferred. This is in part due to the relatively large increments in updraft intensity between simulations (recall the w_{max} steps of [20, 33, 45] m s^{-1}). Updraft intensity is expected to increase with higher instability, but updrafts depend on many other factors, such as storm dynamics. Thus, this topic is still rather uncertain and beyond the scope of this study[28,29]. In other words, CC scaling cannot be applied to updraft intensity and updraft width, so there is no way to systematically analyze the impact here. What can be said based on Fig. 3d is that in regions where average updraft kinematics change in the future, the impact on the hail size spectrum is not necessarily monotonic and may overrule thermodynamic changes.

Hail area

The realistic hail trajectories also allow for more detailed analyses than hail size. The area affected by hail, for example, is also important for the damage caused by a hailstorm. Actual hail swaths also depend on the propagation speed and direction of the storm, which are not represented by the fixed updrafts and embryo starting times herein. However, as an approximation of hail swath area, Fig. 5 shows relative changes in the area affected by severe hail. The results are qualitatively similar to the changes in the hail sizes above. Warming by 3 K leads to an average reduction in area by −3% and moistening to an increase in area by 29%. The combined effect is dominated by the water vapor increase. Updraft width shows the largest positive trend around 40–60%, while updraft intensity shows mixed trends as expected from the diverging signal in Fig. 3d. These signals are similar when using different thresholds for hail size or the minimum number per gridpoint, but tend to decrease in magnitude for smaller hail.

Underlying hail growth mechanisms

The full 3D hail trajectories provide the opportunity to analyze the physical reasons for the trends shown above. To keep the storage space at a reasonable level, the full trajectories were only saved if the hailstones reached a maximum diameter of at least 3 cm at the ground. Thus, smaller sizes are not included in the following analysis.

We arbitrarily pick one control simulation from the center of the parameter space defined by a surface potential temperature of 297 K, water vapor mixing ratio of 13 g kg^{-1}, and the moderate updraft intensity and width used herein. This simulation is then compared to the "neighboring" simulations in our parameter space, i.e., one simulation 3-K colder and one 3-K warmer, and vice versa for water vapor, updraft intensity, and updraft width. Figure 6 shows that each of these simulation triplets behaves as expected from the previous sections. Increasing melting level leads to fewer severe hailstones; increasing water vapor or updraft width leads to more severe hail, and moderate updraft intensity shows a peak in hail production. Thus, any physical processes found for this subset of simulations are likely representative of the whole ensemble.

To understand the underlying processes that lead to the observed changes in the hail size spectrum, Fig. 7 shows violin plots of relevant quantities of the hail trajectories. As expected for the simulations with higher temperature and higher melting levels (orange violins), a larger fraction of the hailstones melts before reaching the ground (Fig. 7a). However, melting alone cannot explain the decrease in surface hail of 3 cm or larger, because the maximum hail size reached per trajectory, i.e., prior to melting, also decreases with higher temperatures (not shown). In addition to melting, there is a dynamic affect of rising melting levels. In warmer conditions, hail embryos start and grow at higher altitudes on average, because there are fewer embryos from low altitudes that make it into the updraft core before melting (Fig. 7b). At higher altitudes, the horizontal and vertical velocity in the updraft are larger, causing an average reduction in residence time of hail in the updraft core (Fig. 7c, e, f).

An increasing water content in the simulations (blue violins) also leads to a reduction in the average residence time for the same reasons. This is because more latent heating results in higher in-updraft temperatures and therefore a shift in the supercooled water maximum to higher altitudes. However, this negative effect on hail size is apparently offset by the increase in hail growth rates in the moister clouds (Fig. 7d). As a result, the amount of

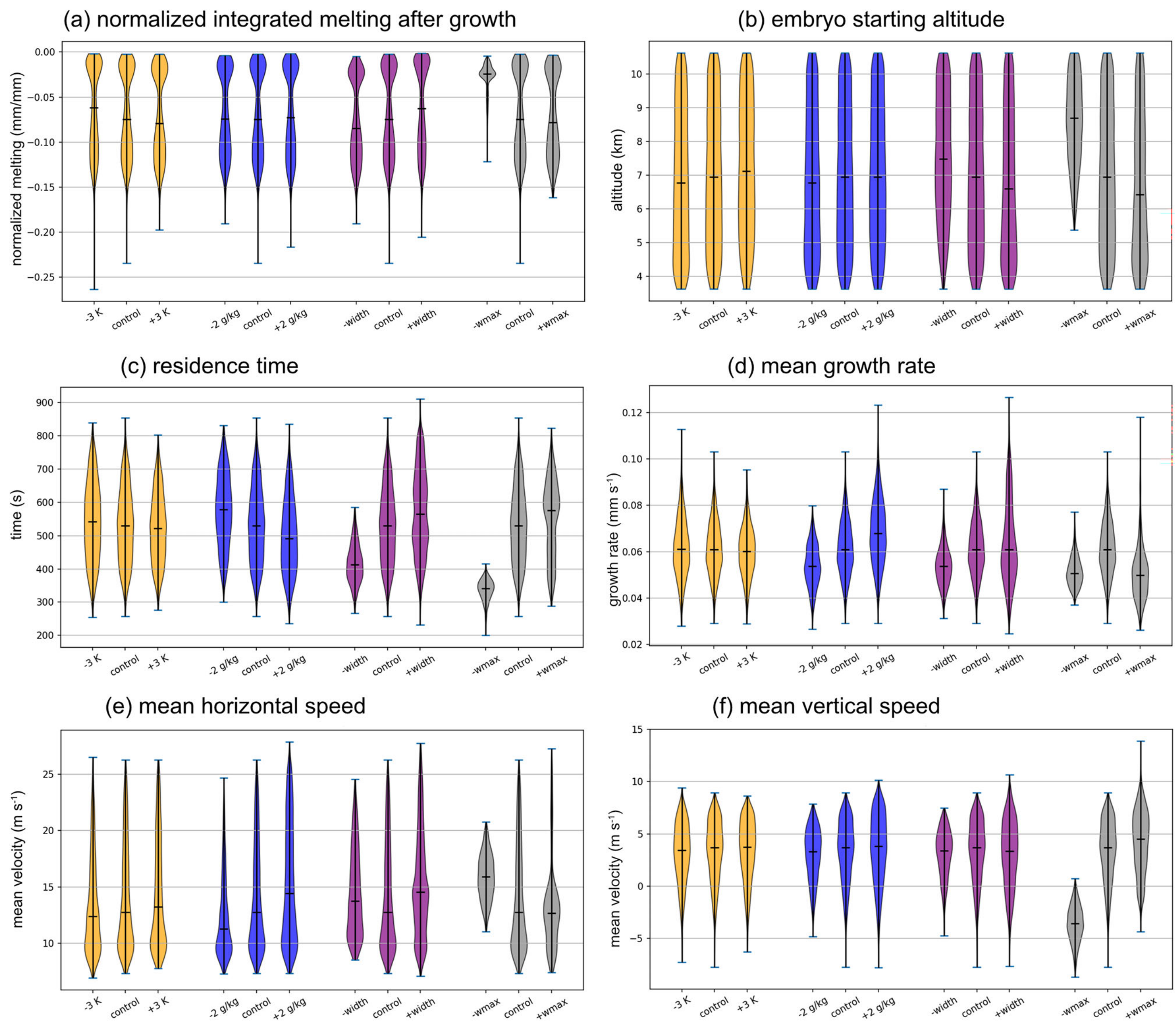

Fig. 7 | Processes along the trajectories. For the same simulations as in Fig. 6, each plot shows the violin plot distribution of the following quantities calculated from the individual hail trajectories. **a** Integrated negative growth after leaving the updraft normalized by the maximum size, i.e., the fraction of the hail maximum dimension that melted after leaving the updraft, **b** starting altitude of the hail embryo, **c** residence time within the> 10 m s^{-1} updraft, **d** mean growth rate over all timesteps with growth, **e** mean horizontal speed and **f** mean vertical speed of the hailstone within the updraft (updraft velocity> 10 m s^{-1} linearly interpolated from the model grid).

hail of almost all sizes increases with larger water content, except for hail <1 cm (Fig. 3b). The reason for the decrease in very small hail could not be isolated in this analysis. However, one possible reason is that, theoretically, melting rates increase with larger absolute moisture in the environment[30], although this is not evident for the severe hail analyzed in Fig. 7. Another possible explanation is that the size distribution simply shifts to larger sizes, so that the decrease in small hail is more of a statistical artifact. However, similar shifts in the size spectrum due to limited embryo availability (or due to limited cloud water availability that was considered limitless herein) might also occur in real storms.

The most important impact of updraft width (violet violins) is the increase in the residence time (Fig. 7c). Furthermore, slower melting and increasing growth rates seem to contribute to the increase in the amount of severe hail. This suggests a shift in the average trajectory pathway with increasing updraft width, consistent with F25. The average trajectory starts at a lower altitude (Fig. 7b), spends more time in the updraft core, and falls in a different region relative to the updraft.

Regarding updraft intensity (gray violins), moderate vertical velocities are optimal because the hail trajectories can move closer to the updraft core (Fig. 7d) while also maintaining sufficient residence time (Fig. 7c). This is not possible in stronger updrafts, because the trajectories avoid the updraft core where they would be vertically ejected (Fig. 7f; see also F25). The increasing residence time as hail trajectories curve around the updraft flank is dwarfed by the reduction in growth rate due smaller cloud water content than in the updraft core (Fig. 7c, d). In weaker updrafts on the other hand, the terminal fall velocity is not balanced, meaning that hail directly falls to the ground (Fig. 7c, f; see also F25). Three side effects of these trajectories are that (i) only hail embryos that start at high altitudes can trace a sufficiently long path through the updraft to grow to severe hail size (Fig. 7b), (ii) the hail falls to the ground almost directly under the updraft (see F25), and (iii) the horizontal hail speed is larger in the weaker updrafts because the >10 m s^{-1} threshold used in Fig. 7e is only reached at higher altitudes.

Overall, these results explain the systematic changes in the hail size distributions in Fig. 3 and make physical sense, which is reassuring. One difficulty for the interpretation is perhaps that the hail size ranges and number of hailstones in these statistics are imbalanced between simulations (Fig. 6) and dominated by smaller sizes (Fig. 2). To assess this uncertainty, we repeated the analysis for two trajectory subsets. In a subset that considers only the 500 largest hailstones per simulation, the differences become more pronounced for most quantities, especially growth rate and residence time, but the trends are the same as above. In a subset using only the starting embryos that are found in all three simulations, i.e., the embryos that reached greater than 3 cm in maximum diameter, some distributions change drastically and become difficult to interpret, because the same embryo might take a completely different path through the updraft. However, for the simulations with varying temperature or moisture in which the flow is comparable, the results are consistent with the findings above.

Figure 1 shows this for a representative embryo starting around 8.2 km above ground. All trajectories experience some initial melting while entering the updraft below the melting level. Compared to the control run (black circles), the trajectory in the 3-K warmer simulation (orange circles) melts slightly more at this time, causing it to be lighter and carried higher aloft. Growth rates in the updraft core are comparable between these two simulations, but the hailstone starts to melt earlier, both because it is carried further outside the updraft by the stronger horizontal winds aloft and because the melting level is a few hundred meters higher than in the control run. The moister simulation (blue circles) shows much larger growth rates than the control run, but a resulting earlier drop out of the updraft core.

Discussion

We find that rising melting levels associated with 3-K warming (without changes in lapse rate) result in less hail of most sizes for two reasons: (i) more melting and (ii) hail forming at higher altitudes in storms, where residence time is reduced because of faster horizontal and vertical advection. However, environmental water vapor increases in line with Clausius-Clapeyron scaling (13–22% per 3-K warming) offset the melting for hail >1.5 cm, resulting in average +30 to +40% increases in the amount of severe and significantly severe hail and +25% increase in the area affected by severe hail. The main reason is the faster growth rate of hail due to more supercooled cloud water. We stress the important role of supercooled water content since it has received less attention than rising temperatures and instability[7]. Nevertheless, the fact that these detailed hail model results are largely consistent with the literature is reassuring and lends robustness to the expected increase in severe hail frequency under climate change.

However, we also find that changes in updraft width and intensity are similarly or more impactful for the hail size spectrum and for the hail footprint than the thermodynamics above. Wider updrafts cause the largest increases in severe hail and larger hail in this study, a role that is consistent with the literature[22,23]. Many studies assume that larger instability in a warmer atmosphere creates stronger updrafts that produce more severe hail[7]. Our detailed hail trajectories do not confirm this chain of thought for supercell storms [see also Ref. 31], except perhaps when only considering giant hail (see F25). Moderate updrafts (around 30 m s^{-1} maximum vertical velocity in the hail growth zone) are optimal for severe and significantly severe hail trajectories, although the steady-state updraft approach and the terminal velocity parameterization might exaggerate this result, as discussed below. Another explanation could be that the stronger updrafts still produce similarly-sized hail, just in smaller quantities, as hail trajectories only travel along the periphery of the updrafts. Such details like hail quantity and area are not well represented in most studies with simpler hail diagnostics, which often just use a deterministic view on hail occurrence.

Unfortunately, it is difficult to make predictions for real climate change based on these results because updraft characteristics are not only a function of thermodynamics associated with CC scaling. Changes in storm organization and updraft structure are highly uncertain and regionally dependent[7] [29]. What can be said is that in regions typically characterized by a lack of instability, the increase in hail is expected to be most pronounced, because intensifying updrafts positively contribute to hail growth. This could explain why instability-limited regions like parts of Europe show the largest increase in hail potential[1] and why the range of hail sizes that are increasing is larger for Europe than the USA[11,13]. However, these studies have very different approaches and do not fully resolve supercell structure, so there are other possible reasons for these different outcomes.

During the review stage of this article, the study of Ref. 32 was published, whose approach bears similarities to our study. They modeled hail trajectories across a wider range of global environments than possible herein, but both their hail trajectory model and their parameterized updrafts were more idealized. We see both approaches as complementary. For example, they show a transition from decreasing to increasing hail around the 1.5 cm mark in mid-latitude regions, which fits our results remarkably well (Fig. 4a). They also noted an increase in the altitude of the hail growth layer, consistent with the result that rising melting levels had a dynamic effect on the hail trajectories herein. We believe these interesting findings show the potential of such hail trajectory modeling studies compared to traditional approaches.

We acknowledge that the present study has several limitations, which result in considerable uncertainty in the results. On the trajectory model side, recent studies have found deficiencies in the commonly used parameterizations of terminal fall velocity[33] and melting[30]. The optimal updraft intensity range, the bimodal distribution in the melting rates (Fig. 7a), and the gap in hail size spectrum between 0.5 and 1 cm (Fig. 2) can likely be attributed to these parameterizations, as explained in the Methods section. Regarding caveats of the idealized supercell updrafts, it is important that the updrafts are steady-state, that high-end updrafts were excluded, and that the moisture fields were decoupled from the CM1 simulation. These aspects are also discussed below. Other simplifications include the missing variability in wind shear (which we chose to omit as it is still uncertain or secondary for hail under climate change[7]), constant lapse rates and relative humidity aloft (which might change in dry regions[34]), the abundant embryos seeded, and that hydrometeor fields were set to zero. Most of these simplifications were necessary to isolate the individual roles of cloud water, melting level, and updrafts in this study. Given that all studies on hail under climate change have weaknesses, we still see the unique, detailed trajectory approach used herein as an important additional perspective.

It is also emphasized that the results focus on process understanding for a fixed ensemble of storms in a warmer climate. In other words, they are independent of storm initiation and thus storm frequency on the occurrence of hail. In regions where storm frequency is expected to decrease, for example due to drier conditions with more convective inhibition like over southwest Europe[13], the associated hail frequency changes are also relevant. *To work towards understanding more and more regional trends in hail occurrence, changes in storm frequency and structure need to be considered, not just thermodynamics in the storm environment.* Future studies linking climate change and hail could also focus on model-resolution dependence, as well as comparing and improving hail diagnostics.

Methods

Idealized simulation ensemble

The idealized supercell-like updrafts in F25 are used as a basis for the simulations in this study. Essentially, we transport this ensemble of updrafts into altered climate conditions to assess whether warmer or moister environments systematically affect hail production.

F25 introduced 25 idealized updrafts with independently changing updraft intensity and updraft width. The updrafts were simulated using the Cloud Model 1 [CM1[35]] employing a highly idealized framework in which a heat source directly controls magnitude and spatial extent of convective heating and thus updraft intensity and width. Furthermore, the trajectory model uses steady-state updrafts as input, so the simulated updrafts were averaged over 20 min as explained in F25. This mean-state approximation removes features like updraft pulses or vortex shedding, which contribute to hail formation in real storms[36–38]. However, since our study focuses on average changes in hail production due to climate change, we argue that the mean-state approximation is sufficient to represent the mean hail production of a storm (see discussion in F25). The simulations have a horizontal resolution of 500 m and a vertical resolution of 250 m, which is linearly interpolated to 300 m and 175 m after the temporal averaging to improve the density and accuracy of hail trajectories. The wind profile is a quarter-circle hodograph in all simulations.

As discussed below, we found that hail production diminished in the strongest updrafts when using the more realistic trajectory model compared to the spherical hail model used by F25. Furthermore, wider updrafts show a monotonically increasing impact on hail size. Thus, no changes in the overall results are expected when excluding these extreme cases. To limit computational expense, only a subset of the 25 updraft simulations is therefore used, removing the two most intense and widest updraft steps, which likely only represent extreme cases. The updraft widths and intensities used represent values that are expected to be common in real supercells [Ref. 39, see also F25]: maximum vertical velocities of [20, 33, 45] ±1 m s^{-1} and updraft areas (gridpoints with >5 m s^{-1} at 5 km) of [36, 56, 80] ±2 km^2, with ± indicating the variability in the nine simulations. As an example, the dashed black lines in Fig. 8 illustrate the maximum vertical velocity with height for the three updraft intensity levels used and with fixed ~80 km^2 updraft area. We refer to F25 for more details on the three-dimensional updraft structure and CM1 simulation setup.

In addition to the range of updraft intensity and width, we independently perturb (a) the melting level height and (b) the near-ground water vapor mass fraction. For (a), the whole temperature profile used by F25 is shifted in 3-K increments with the surface potential temperature set to [291, 294, 297, 300, 303] K, respectively. To maintain computational feasibility, these temperature perturbations are applied in post-processing over the whole domain rather than by rerunning the simulations. Hydrostatic pressure and density are adjusted accordingly. This simple method is only possible because the simulations are effectively temperature-invariant over this range because (i) the idealized updrafts are driven solely by the heat source with no feedbacks between temperature, moisture, and microphysics as in full-physics simulations and (ii) only steady-state updrafts are used, so local variations in the updraft are averaged out. While this simplification may introduce minor differences compared to rerunning the simulation, this is not expected to change the results. Therefore, it is considered acceptable given that it reduces the required number of simulations by a factor of five. The five different temperature profiles represent increasing melting level heights between 2.5 and 5.5 km (the exact heights also depend on latent heating within the different updrafts), consistent with midlatitude hail environments[40].

The liquid water and ice fields within the updraft needed for the trajectory model are also added in post-processing. We improved the method used by F25, in which moisture fields were copied from the microphysics scheme in a separate full-physics supercell simulation. Instead, the cloud water and ice content in the updraft core are now derived from pseudoadiabatic parcel ascent, based on the argument that supercell updraft cores are nearly adiabatic[39,41]. Parcel ascent calculations follow the methodology described in Ref. 42, with the transition of cloud water from liquid to ice phase set to the temperature range −25 to −38 °C following Ref. 40. The entrainment rate is set to zero for the updraft core parcel, but the precipitation rate is set to 0.05 km^{-1} to allow for some reduction of the total water content with height. A mixed-layer parcel of the lowest 200 m is used for the parcel ascent to allow for a layer with large moisture. With the described procedure, near-ground moisture can be changed as the fourth independent parameter, with water vapor mass fraction values set to [9, 11, 13, 15, 17] g kg^{-1}, respectively (Fig. 8). These values span water vapor concentrations observed near midlatitude supercells[40,43]. Above 200 m, environmental relative humidity is fixed at 50%. It is impossible to represent the range of relative humidity values and vertical variability that can exist in the free atmosphere, but we see this moderate humidity as a reasonable compromise[44].

As shown in Fig. 8, the pseudoadiabatic parcel ascent produces a realistic vertical profile of liquid cloud and ice water mixing ratios for each combination of parcel potential temperature and water vapor mass fraction. To expand these one-dimensional profiles onto the three-dimensional simulated updrafts while accounting for entrainment, we follow a similar procedure to that of Ref. 22. The mixing ratio profiles are applied to all gridpoints with >95% of the maximum updraft at the same height. Outside this updraft core, the mixing ratios are reduced parabolically based on the fraction of vertical velocity to updraft core velocity. All gridpoints with <2 m s^{-1} vertical velocity are set to zero cloud liquid and ice mixing ratios. Mixing ratios and number concentrations of rain, snow, and graupel are not included in this approach and are set to zero everywhere. This decision was based on the sensitivity tests in F25, which showed negligible influence of snow and graupel concentrations, and only some contribution of rain, and only towards larger hail. Thus, higher rainwater content could further increase the positive trends in severe hail with increasing absolute humidity found herein, but likely not change the overall results.

The procedure above implies that the theoretical vertical velocity predicted by the parcel ascent is neglected and that the actual updraft is prescribed by the simulations. Figure 8 shows that the differences in the vertical velocities of the theoretical parcel and the simulations can be substantial. Strictly speaking, this means that combining the simulated updrafts and the moisture fields in this decoupled manner is unphysical because (i) the temperature in the updraft is not adjusted when moister parcels ascend with more latent heating. This, for example, leads to artificial shifts of the melting level by up to 1 km (although just a few hundred meters in most cases), meaning that cloud water and ice concentrations do not match the expected temperature ranges. Given that the temperature ranges for water-ice transition and hail growth are uncertain in the first place, we argue that this caveat is acceptable. In terms of how it affects the results, the increase in water content at higher altitude seems to have a mostly negative effect on average residence time (Fig. 7c). This means that the water vapor effect on hail size is perhaps underestimated, but the general trend of increasing hail with larger water content is robust. (ii) The theoretical parcel vertical velocity does not match the simulated updrafts (Fig. 8), which also means that in some cases extremely high cloud water contents are modeled in weak updrafts, which is likely physically impossible. A sensitivity test by repeating the analysis only using simulated updrafts that were within 50–200% of the maximum predicted parcel vertical velocity (105 of 171 cases) showed no changes in the results. The tested percentage range is still quite large, but since limited observations exist of within-storm quantities to conclude what combinations of updraft speeds and water contents are realistic, this topic is beyond the scope of this paper. Furthermore, we argue that real storms are also not well represented by parcel theory, owing to effects such as entrainment, pressure perturbations, or storm interactions. In other words, real storms likely exist with most of the combinations of updrafts and mixing ratios shown in Fig. 8, so the ensemble is sufficiently realistic for the purposes of this study (see discussion).

Another simplification is that the updrafts herein are constant with time based on the argument that these average updrafts represent the average, most common hail trajectories in real storms. It is possible that more complex trajectories make up the majority of hail in real storms[37,38], which would reduce the representativeness of the results herein. However, most of the physical processes shown likely also affect more complex trajectories.

The idealized, computationally inexpensive methods described above are necessary for two reasons. First, real supercells exist over a large spectrum of intensities, shapes, temperature ranges, and water contents. Thus, a large number of simulations is required to apply the findings to real climate change scenarios. Second, as discussed in detail by F25, full physics simulations of storms often react nonlinearly to changes in the environment, e.g., an increasing water vapor content affecting microphysics and downdraft structure. Here, our goal is to systematically test hail production response to each variable independently, which is possible with the idealized setup and fixed storm structure.

In summary, this methodology of independently varying updraft intensity (3 steps), updraft width (3 steps), potential temperature (5 steps), and water vapor content (5 steps) results in an ensemble of 3 × 3 × 5 × 5 = 225 simulations. Of these, 54 simulations are excluded because their combinations of temperature and water vapor mass fraction produce unphysical parcel ascents. This can be either because the parcels are supersaturated near the surface at low temperatures (missing plots in the top-left corner of Fig. 8) or because the parcels never become positively buoyant in hot and dry

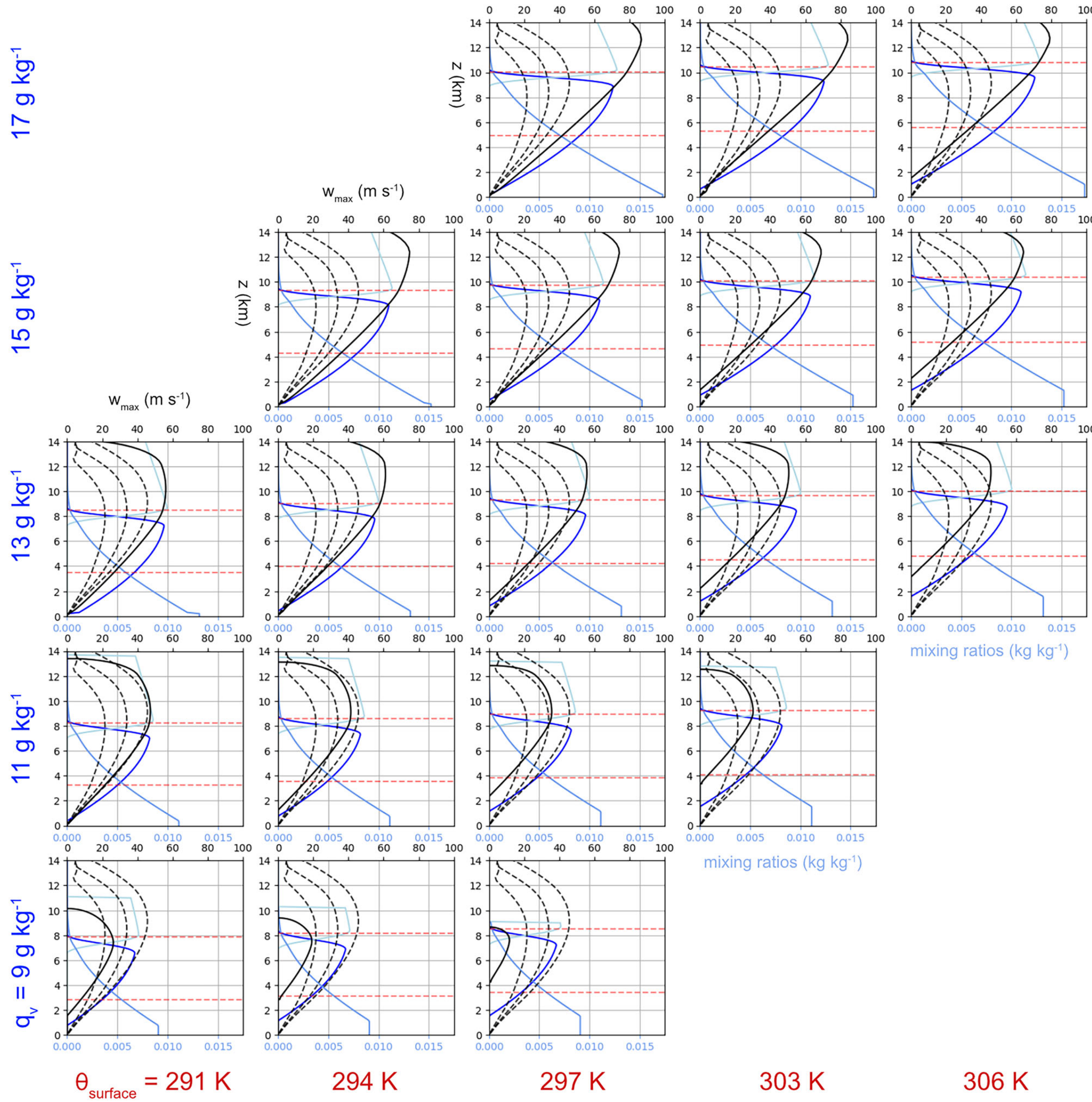

Fig. 8 | Overview over the parameter space of the simulation ensemble. For each combination of surface potential temperature and water vapor mass fraction, the respective subplot shows the pseudoadiabatic parcel ascent described in the text, with parcel water vapor mixing ratio (sky blue), cloud water mixing ratio (dark blue), ice mixing ratio (light blue), and integrated vertical velocity (black, second x-axis). The maximum vertical velocity profile for the three simulations with different heat source intensities is also shown (dashed black). Dashed red lines indicate the 0 °C level and the −38 °C level of the parcel.

conditions (bottom-right corner). This results in a final ensemble of 171 simulated steady-state updrafts, which serve as input for the hail trajectory model.

Trajectory model

The [Ref. 45, hereafter L24] version of the Kumjian and Lombardo hail trajectory model[46] is used, in which individual hailstone trajectories are calculated in 1-s time steps. This trajectory model version includes the effects of nonspherical hailstone shapes, tumbling, surface roughness, wet and dry growth, and melting. The settings recommended by L24 are used, which include explicit tumbling of each hailstone, a randomly set aspect ratio, and explicit calculation of the drag coefficient and terminal velocity[47,48]. The heat transfer coefficient is adjusted with the aspect ratio. Lobes are not modeled to reduce computational costs, as lobes were found to only have a secondary effect on hail size in L24.

Several additional modifications are made to the trajectory model. Previous studies using this model mainly seeded embryos in a region covering the whole updraft [e.g., Ref. 46, F25]. However, these studies typically found that, at least in steady-state updrafts, the majority of hailstones originate southwest of the updraft, consistent with the embryo curtain in real supercells[49]. To reduce computation time for the large number of simulations in the present study, the embryos are only seeded in this dominant region. Specifically, the embryos are started at every model gridpoint within $-9 \le x \le 6.3$ km, $-10.8 \le y \le 4.2$ km, $3.625 \le z \le 10.625$ km, resulting in a total of 108 732 hail trajectories for each simulation. All simulations were checked manually to ensure that the main source region of hail was within this box. To avoid having to run the model repeatedly for different hail embryo sizes, the starting embryo size is selected randomly between 2 and 10 mm. The mass density of each embryo is also varied randomly within the range of 500 to 917 kg m^{-3} to represent soft and porous graupel as well as frozen raindrops. Real hail embryo sizes and densities are likely not uniformly distributed, but there is high uncertainty with respect to hail embryos, so this methodology seems sufficient to allow for some variability[46]. The same random embryos are used across the whole ensemble. As an example, Fig. 1 shows the trajectories of the same embryo in three different simulations.

Despite this being the most advanced hail trajectory model currently available, L24 states that "significant uncertainty remains in some aspects (e.g., falling behavior)." A reason for the penalization of strong updrafts in this study is the large sensitivity of the trajectories to the terminal velocity parameterization. Recent wind tunnel experiments with natural hailstones[33] found that the commonly used parameterizations underestimate terminal velocity and therefore may fail to balance out strong updrafts. This likely did not affect the main results of this study since the optimal updraft spectrum was merely shifted, but future studies with hail trajectories and varying updraft intensities should consider this aspect.

Furthermore, hail trajectory models commonly assume that the hailstone surface is in thermal energy balance with the environment at every simulated time. When hailstones enter the melting phase from the dry growth phase, the instantaneous thermal energy balance transfer can result in a sharp jump of simulated hail size. There are two unexpected behaviors in the modeled hailstones that can be linked to this effect. (i) The bimodal distribution in the melting rates (Fig. 7a) separates hailstones that enter the melting phase from dry or wet growth. Hailstones without surface liquid water instantaneously melt the complete outer hailstone layer and thus have much larger integrated melting. (ii) The gap in hail sizes between 0.5 and 1 cm (Fig. 2) can likely be attributed to small hail with just one layer of dry growth that melts instantaneously. The chosen starting embryo sizes between 2 and 10 mm could also play a role here. This gap increases the uncertainty in the results for hail smaller than 1 cm. On the other hand[30], showed that small hail often completely melts in tropical environments, which is consistent with the results herein. Their study also emphasizes the general uncertainty in melting parameterizations. For example, despite its common usage, the validity of the thermal energy balance assumption above remains unexamined. These aspects of the trajectory model are planned to be validated and improved.

Data availability

The model fields and hail trajectories required to reproduce the results are published (https://doi.org/10.35097/0ksm5m6nre3nvbcb).

Received: 1 June 2026; Accepted: 15 August 2026;
Published online: 07 September 2026

References

1. Battaglioli, F., Taszarek, M., Groenemeijer, P., Púčik, T. & Rädler, A. Contrasting trends in very large hail events and related economic losses across the globe. *Nat. Geosci.* **19**, 52–59 https://doi.org/10.1038/s41561-025-01868-0 (2026).
2. Trapp, R. J. et al. Changes in severe thunderstorm environment frequency during the 21st century caused by anthropogenically enhanced global radiative forcing. *Proc. Natl. Acad. Sci. USA* **104**, 19719–19723 https://doi.org/10.1073/pnas.0705494104 (2007).
3. Diffenbaugh, N. S., Scherer, M. & Trapp, R. J. Robust increases in severe thunderstorm environments in response to greenhouse forcing. *PNAS* **110**, 16361–16366 https://doi.org/10.1073/pnas.1307758110 (2013).
4. Mohr, S., Kunz, M. & Keuler, K. Development and application of a logistic model to estimate the past and future hail potential in Germany. *J. Geophys. Res.: Atmos.* https://doi.org/10.1002/2014JD022959.Abstract (2015).
5. Rädler, A. T., Groenemeijer, P. H., Faust, E., Sausen, R. & Púčik, T. Frequency of severe thunderstorms across Europe expected to increase in the 21st century due to rising instability. *npj Clim. Atmos. Sci.* **2**, 3–7 https://doi.org/10.1038/s41612-019-0083-7 (2019).
6. Lepore, C., Abernathey, R., Henderson, N. & Allen, J. T. Future global convective environments in cmip6 models: Earth's future. *Earth Future* **9**, 1–21 https://doi.org/10.1029/2021EF002277 (2021).
7. Raupach, T. H. et al. The effects of climate change on hailstorms. *Nat. Rev. Earth Environ.* 32–36 https://doi.org/10.1038/s43017-020-00133-9 (2021).
8. Wang, Z., Franke, J. A., Luo, Z. & Moyer, E. J. Reanalyses and a high-resolution model fail to capture the "high tail" of CAPE distributions. *J. Clim.* **34**, 8699–8715 https://doi.org/10.1175/JCLI-D-20-0278.1 (2021).
9. Manzato, A., Fasano, G., Cicogna, A., Sioni, F. & Pucillo, A. Relationships between environmental parameters and storm observations in Po Valley: Are they climate change invariant? *J. Appl. Meteorol. Climatol.* **64**, 267–298 https://doi.org/10.1175/JAMC-D-24-0034.1 (2025).
10. Chericoni, M., Fosser, G., Anav, A. et al. Divergent European hail projections from machine learning and physically based models under global warming. *npj Nat. Hazards* **3**, 58 https://doi.org/10.1038/s44304-026-00218-3 (2026).
11. Gensini, V. A. et al. Hailstone size dichotomy in a warming climate. *npj Clim. Atmos. Sci.* **7**, 1–10 https://doi.org/10.1038/s41612-024-00728-9 (2024).
12. Kumjian, M. R. et al. Gargantuan hail in Argentina. *Bull. Am. Meteorol. Soc.* **101**, E1241–E1258 https://doi.org/10.1175/BAMS-D-19-0012.1 (2020).
13. Thurnherr, I., Cui, R., Velasquez, P., Wernli, H. & Schär, C. The effect of 3 °C global warming on hail over Europe. *GRL* https://doi.org/10.22541/au.173809555.59545480/v1 (2025).
14. Kahraman, A., Kendon, E. J., Fowler, H. J. & Short, C. J. Future changes in severe hail across Europe, including regional emergence of warm-type thunderstorms. *Nat. Commun.* **16**, 1–14, https://doi.org/10.1038/s41467-025-62780-0 (2025).
15. Brimelow, J. C., Burrows, W. R. & Hanesiak, J. M. The changing hail threat over North America in response to anthropogenic climate change. *Nat. Clim. Change* **7** https://doi.org/10.1038/NCLIMATE3321 (2017).
16. Trapp, R. J., Hoogewind, K. A. & Lasher-Trapp, S. Future changes in hail occurrence in the United States determined through convection-permitting dynamical downscaling. *J. Clim.* **32**, 5493–5509 https://doi.org/10.1175/JCLI-D-18-0740.1 (2019).
17. Mahoney, K., Alexander, M. A., Thompson, G., Barsugli, J. J. & Scott, J. D. Changes in hail and flood risk in high-resolution simulations over Colorado's mountains. *Nat. Clim. Change* **2**, 125–131 https://doi.org/10.1038/nclimate1344 (2012).
18. Mallinson, H., Lasher-Trapp, S., Trapp, J., Woods, M. & Orendorf, S. Hailfall in a possible future climate using a pseudo–global warming approach: Hail characteristics and mesoscale influences. *J. Clim.* **37**, 527–549 https://doi.org/10.1175/JCLI-D-23-0181.1 (2024).
19. Trapp, R. J., Lasher-Trapp, S. G., Claybrooke, R. D. & Romppainen-Martius, O. A storyline climate-change attribution study of a high-impact hailstorm in Switzerland. *Geophys. Res. Lett.* **52** https://doi.org/10.1029/2025GL117142 (2025).
20. Lucas, L., Barthlott, C., Hoose, C. & Knippertz, P. Aerosol effects on convective storms under pseudo-global warming conditions: insights from case studies in Germany. *Atmos. Chem. Phys.* **25**, 18527–18548 https://doi.org/10.5194/acp-25-18527-2025 (2025).
21. Blair, S. F. et al. High-resolution hail observations: Implications for NWS warning operations. *Weather Forecast.* **32**, 1101–1119 https://doi.org/10.1175/WAF-D-16-0203.1 (2017).
22. Nelson, S. P. The influence of storm flow structure on hail growth. *J. Atmos. Sci.* **40**, 1965–1983 https://doi.org/10.1175/1520-0469(1983)040%3C1965:TIOSFS%3E2.0.CO;2 (1983).
23. Dennis, E. J. & Kumjian, M. R. The impact of vertical wind shear on hail growth in simulated supercells. *J. Atmos. Sci.* **74**, 641–663 https://doi.org/10.1175/JAS-D-16-0066.1 (2017).

24. Weisman, M. L., Skamarock, W. C. & Klemp, J. B. The resolution dependence of explicitly modeled convective systems. *Mon. Weather Rev.* **125**, 527–548 https://doi.org/10.1175/1520-0493(1997)125%3C0527:TRDOEM%3E2.0.CO;2 (1997).
25. Prein, A. F., Wang, D., Chasteen, M. B., Ge, M. & Valle, A. R. Resolving mesoscale convective systems: Grid spacing sensitivity in the tropics and midlatitudes. *JGR Atmos.* https://doi.org/10.1029/2024JD042530 (2025).
26. Fischer, J., Kunz, M., Lombardo, K. & Kumjian, M. R. Hail trajectories in a wide spectrum of supercell-like updrafts. *J. Atmos. Sci.* **82**, 1403–1422 https://doi.org/10.1175/JAS-D-24-0222.1 (2025).
27. Held, I. M. & Soden, B. J. Robust responses of the hydrological cycle to global warming. *J. Clim.* **19**, 5686–5699 https://doi.org/10.1175/JCLI3990.1 (2006).
28. Peters, J. M., Chavas, D. R., Lebo, Z. J. & Su, C.-Y. Cumulonimbus clouds convert a smaller fraction of CAPE into kinetic energy in a warmer atmosphere. *J. Atmos. Sci.* 1943–1961 https://doi.org/10.1175/jas-d-24-0006.1 (2024).
29. Feldmann, M. et al. European supercell thunderstorms—a prevalent current threat and an increasing future hazard. *Sci. Adv.* **11**, 1–12 https://doi.org/10.1126/sciadv.adx0513 (2025).
30. Vagasky, H. C., Adams-Selin, R. D., Bang, S. D., Heymsfield, A. J. & Bansemer, A. The sensitivity of falling hail to different melting and terminal velocity parameterizations and environmental conditions. *Mon. Weather Rev.* **153**, 2535–2554 https://doi.org/10.1175/MWR-D-24-0180.1 (2025).
31. Lin, Y. & Kumjian, M. R. Influences of CAPE on hail production in simulated supercell storms. *J. Atmos. Sci.* **79**, 179–204 https://doi.org/10.1175/JAS-D-21-0054.1 (2022).
32. Zhang, S., Zhang, Q., Allen, J. T. & Lin, X. Rising global hail damage potential in a warming world. *Nature* **653**, 1069–1077 https://doi.org/10.1038/s41586-026-10543-2 (2026).
33. Theis, A., Voll, L., Diehl, K., Heymsfield, A., Giammanco, I., Borrmann, S., & Szakáll, M. A Wind Tunnel Investigation into the Aerodynamics of Natural Hailstones. *J. Atmos. Sci*., **83**, 927–942, https://doi.org/10.1175/JAS-D-25-0015.1 (2026).
34. Brogli, R., Sørland, S. L., Kröner, N., Schär, C. & Pole, S. Future summer warming pattern under climate change is affected by lapse-rate changes. *Weather Clim. Dyn.* 1093–1110 https://doi.org/10.5194/wcd-2-1093-2021 (2021).
35. Bryan, G. H. & Fritsch, J. M. A benchmark simulation for moist nonhydrostatic numerical models. *Mon. Weather Rev.* **130**, 2917–2928 https://doi.org/10.1175/1520-049 (2002).
36. Kumjian, M. R., Lombardo, K. & Loeffler, S. The evolution of hail production in simulated supercell storms. *J. Atmos. Sci.* **78**, 3417–3440 https://doi.org/10.1175/JAS-D-21-0034.1 (2021).
37. Pounds, L. E., Ziegler, C. L., Adams-Selin, R. D. & Biggerstaff, M. I. Analysis of hail production via simulated hailstone trajectories in the 29 may 2012 Kingfisher, Oklahoma, supercell. *Mon. Weather Rev.* **152**, 245–276 https://doi.org/10.1175/MWR-D-23-0073.1 (2024).
38. Adams-Selin, R. The quasi-stochastic nature of hail growth: Hail trajectory clusters in simulations of the Kingfisher, Oklahoma, hailstorm. *Mon. Weather Rev.* **153**, 67–87 https://doi.org/10.1175/MWR-D-23-0233.1 (2025).
39. Peters, J. M., Morrison, H., Nowotarski, C. J., Mulholland, J. P. & Thompson, R. L. A formula for the maximum vertical velocity in supercell updrafts. *J. Atmos. Sci.* **77**, 3033–3057 https://doi.org/10.1175/JAS-D-20-0103.1 (2020).
40. Spychalla, L. & Kumjian, M. R. An analytic approximation of vertical velocity and liquid water content profiles in supercell updrafts and their use in a novel idealized hail model. *J. Atmos. Sci.* **82**, 2077–2099 https://doi.org/10.1175/JAS-D-24-0233.1 (2025).
41. Davies-Jones, R. P. Discussion of measurements inside high-speed thunderstorm updrafts. *J. Appl. Meteorol. Climatol.* **13**, 710–717 https://doi.org/10.1175/1520-0450(1974)013%3C0710:DOMIHS%3E2.0.CO;2 (1974).
42. Peters, J. M., Mulholland, J. P. & Chavas, D. R. Generalized lapse rate formulas for use in entraining CAPE calculations. *J. Atmos. Sci.* **79**, 815–836 https://doi.org/10.1175/JAS-D-21-0118.1 (2022).
43. Taszarek, M., Allen, J. T., Púčik, T., Hoogewind, K. A. & Brooks, H. E. Severe convective storms across Europe and the United States. Part II: Era5 environments associated with lightning, large hail, severe wind, and tornadoes. *J. Clim.* **33**, 10263–10286 https://doi.org/10.1175/JCLI-D-20-0346.1 (2020).
44. Morrison, H., Peters, J. M., Chandrakar, K. K. & Sherwood, S. C. Influences of environmental relative humidity and horizontal scale of subcloud ascent on deep convective initiation. *J. Atmos. Sci.* **79**, 337–359 https://doi.org/10.1175/JAS-D-21-0056.1 (2022).
45. Lin, Y., Kumjian, M. R., Soderholm, J. & Giammanco, I. Modeling non-spherical hailstones. *J. Atmos. Sci.* 1849–1881 https://doi.org/10.1175/jas-d-23-0231.1 (2024).
46. Kumjian, M. R. & Lombardo, K. A hail growth trajectory model for exploring the environmental controls on hail size: Model physics and idealized tests. *J. Atmos. Sci.* **77**, 2765–2791 https://doi.org/10.1175/JAS-D-20-0016.1 (2020).
47. Heymsfield, A., Szakáll, M., Jost, A., Giammanco, I. & Wright, R. A comprehensive observational study of graupel and hail terminal velocity, mass flux, and kinetic energy. *J. Atmos. Sci.* **75**, 3861–3885, https://doi.org/10.1175/JAS-D-18-0035.1 (2018).
48. Heymsfield, A. et al. Corrigendum. *J. Atmos. Sci.* **77**, 405–412 https://doi.org/10.1175/JAS-D-19-0185.1 (2020).
49. Browning, K. A. & Foote, G. B. Airflow and hail growth in supercell storms and some implications for hail suppression. *Q. J. R. Meteorol. Soc.* **102**, 499–533 https://doi.org/10.1002/qj.49710243303 (1976).

Acknowledgements
We thank Dr. Michael Kunz and Lydia Spychalla for valuable comments. Dr. John Peters is acknowledged for providing code and improvements for the methods. MRK, KL, and YL were supported by grant AGS-2410918 from the U.S. National Science Foundation. J.F.'s position is funded as a Willis Research Fellow, and a research stay during the project was supported by the German Academic Exchange Service (DAAD), both without a grant ID. The funders played no role in study design, data collection, analysis and interpretation of data, or the writing of this manuscript.

Author contributions
J.F. conducted the simulations, analyzed the data, and wrote the manuscript. K.L., Y.L., and M.K. wrote the trajectory model code and provided input and improvements during the planning, analysis, and writing phases.

Funding
Open Access funding enabled and organized by Projekt DEAL.

Competing interests
The authors declare no competing interests.

Additional information
Correspondence and requests for materials should be addressed to Jannick Fischer.